United Nations Educational, Scientific and Cultural Organization
Geothermal Training Programme Under the auspices of UNESCO

GRÓ GTP, Grensásvegur 9,
IS-108 Reykjavík, Iceland

Reports 2021
Number 25

GEOTHERMAL PROPERTIES OF THE THERMAL FLUID FROM BITTUANG, SOUTH SULAWESI, INDONESIA

Widya Asoka Suleman
Center for Mineral, Coal and Geothermal Resources
Geology Agency
Ministry of Mineral and Energy Resources
Jalan Soekarno Hatta no. 444, Bandung
INDONESIA
widya.asoka@gmail.com

ABSTRACT

Eighteen water samples and eleven steam samples were analysed to establish the chemical features, determine the type and origin of the geothermal fluids, and estimate the reservoir temperature in the Bittuang geothermal area in Indonesia. The results of the sample analysis were evaluated using ternary diagrams, binary mixing plots, stable isotope ratios, and geothermometry. The results show that most of the samples are either boiled geothermal water or peripheral waters, the former samples appear to be in a partial equilibrium with the rock and are apparently associated with volcanism. The results of the isotope indicate the contribution of magmatic water also from results of geothermometry suggest reservoir temperatures of 200-260°C, i.e., the presence of a high-enthalpy geothermal system.

1. INTRODUCTION

Indonesia is rich in geothermal resources, with 357 geothermal areas identified along the volcanic belt that comprises Sumatra, Java, Nusa Tenggara, Sulawesi, and Maluku. With a total estimated potential of 23.7 GWe, Indonesia is the world's largest geothermal country in terms of potential and the second largest in term of installed capacity, which amounts to 2131 MWe (Geological Agency, 2020).

This study focuses on the Bittuang geothermal area. Administratively, the Bittuang geothermal area is mostly included in the Tana Toraja Regency area with a small part in the North Toraja Regency, South Sulawesi Province, Sulawesi Island. This study area is located about 25 km northwest of Makale city, the capital of the Tana Toraja Regency (Figure 1). The inset map shows the Sulawesi Island and the bigger map is the enlarged from of the area market in the white box which is South Sulawesi Province. The blackbox shows the region of sata collection which knows as Bittuang geothermal area,

Several researchers have conducted investigations in the Bittuang area, including Bemmelen (1949), Radja (1970), Bachri and Alzwar (1975), and Ratman and Atmawinata (1993) who created a geological map of Mamuju Sheet, West Sulawesi. According to previous studies, geothermal manifestations appear in the form of hot springs, in Bittuang village, Bittuang district. The hot springs have a temperature of around 37°C with a total flow rate of 1 L/s and a pH of 6-7. In addition, there are fumaroles with temperatures between 96-98°C, which have a strong smell of H_2S and give rise to sulfur deposits (Soetoyo, 2010).

The origin of water in the study area will be determined after the chemical and isotope analysis of eighteen samples taken from hot springs and eleven samples taken from fumaroles. The combined geothermometer analysis of hot springs and fumaroles will result in estimation of reservoir temperature in study area.

2. THE STUDY AREA

2.1 Geological overview

The units or stratigraphy from oldest to youngest in Bituang are metamorphic rock (Kbm), sandstone (Tps), Mt. Panusuk lava (TPl), Mt. Ruppu lava (TRl), Rattebombong intrusion (TRbi), Mt. Karua Lava-1 (QKl-1), Mt. Karua-2 (QKl-2), Mt. Karua pyroclastic flow (QKap), Mt. Karua pyroclastic fall (QKjp), Mt. Malibu lava (QMl), and Mt. Karua-3 lava (QKl-3) which is 0.3 million years old (Soetoyo et.al, 2010) as is shown in Figure 2.

In general, there is a pattern of circular features in the form of a horseshoe opening to Mt. Karua the caldera in the north (upper part in Figure 2). There are two dominant lineament patterns in the area trending in NW-SE and NE-SW directions that may have implications for the history of the geology (tectonic and volcanism) and the geothermal systems.

The first lineament is to the west of Mt. Karua where there is a northeast-southwest trending line that can be seen crossing the Karua caldera. This shows that after the period of volcanism that produced the caldera, there was a period of tectonism that produced a northeast-southwest trending structure/fault that cut the Karua caldera. The second lineament south of Mt. Karua is a collection of lineaments trending northwest–southeast and northeast–southwest. The lineaments form a graben pattern which controls the presence of geothermal manifestations in the Bittuang geothermal field (Suleman et al., 2021).

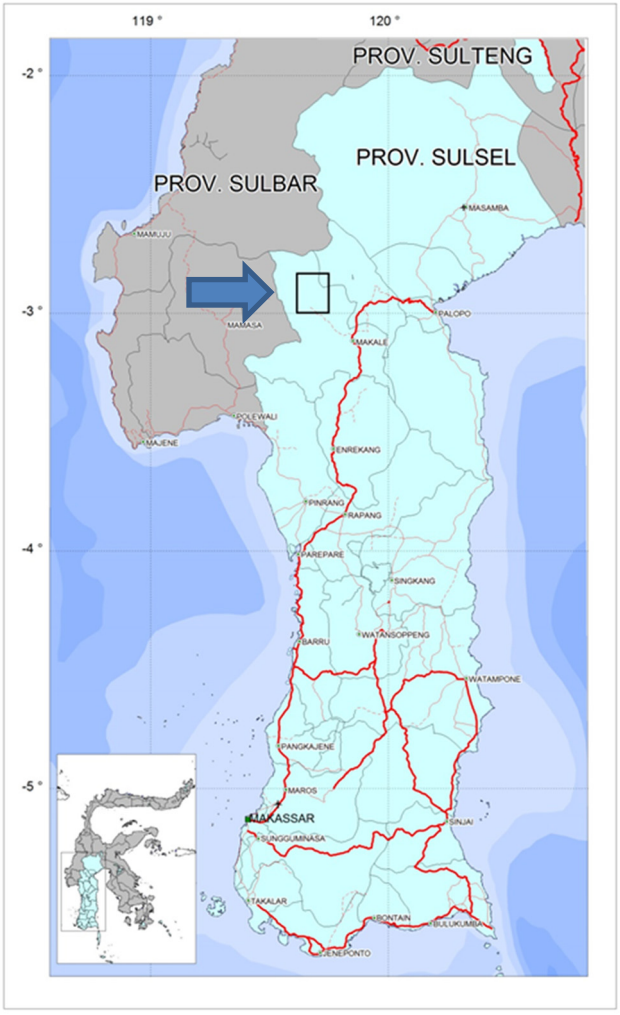

FIGURE 1: Study area map

2.2 Geothermal manifestations

The Bittuang geothermal prospect area has geothermal surface manifestations in the form of hot springs, steam vents, argillic alteration and altered rocks. Hot springs are located around the Balla river, in Kampung Balla and in the Kali Putih River, Kampung Cepeng. The hot springs at the Balla location are accompanied by steam vents. At the locations of these hot springs and steam vents, altered rock can be found.

At the location of the Balla river, there are many hot springs that have temperatures between 36°C and 93°C with a generally very small discharge, less than 0.3 L/s. At least 9 hot springs have been identified near the Balla river. The other manifestations are hot springs in Cepeng, located in the south of the study area (outside of the study area, sample taken for comparison). There are two warm springs in Cepeng that have temperatures of 37.6°C – 39.8°C. An overview of those hot springs is given in Table 1 together with the steam vents and, bubbling hot springs at Balla and bubbling colds springs in the Kaipohan Crater area.

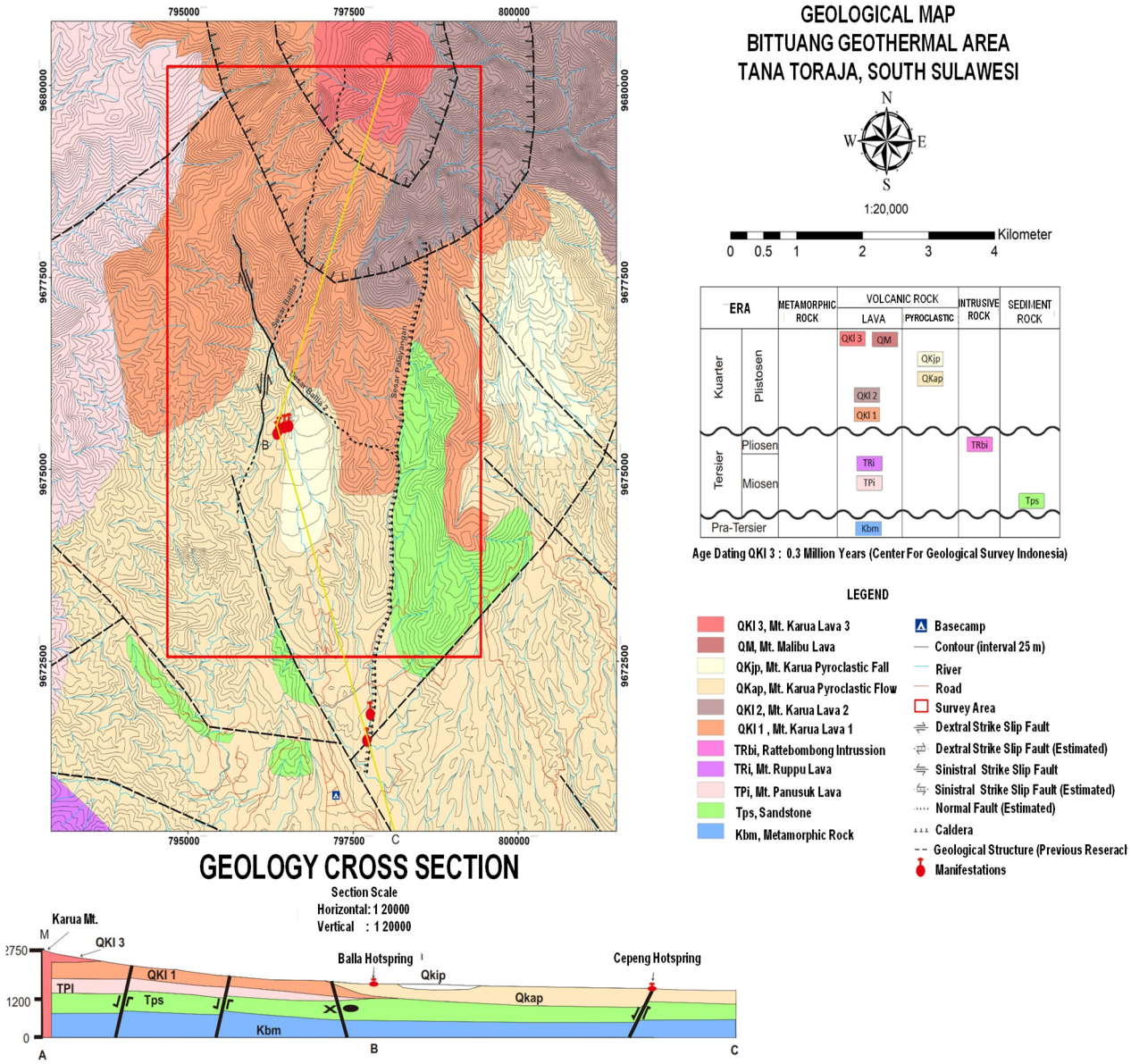

FIGURE 2: Bittuang Geological Map, the study area shown in red box (Suleman et al., 2021)

TABLE 1: Hot Spring in Bittuang (Iim et al., 2021)

MANIFES-TATION	COORDINATE (UTM)		ELEV-ATIO-N	TEMPER-ATURE	pH	FLOW RATE	CONDUC-TIVITY	DESCRIPTION
	X (m)	Y (m)	(m.a.s.l)	(°C)		(L/s)	(µs/cm)	
Air Panas Balla -1 (APB -1)	796405	9675488	1587	71,5	6,2	0,1	6440	Hot spring emerge from the crevice of altered rock on the banks or the Balla River. The water is clear, smells slightly of sulfur and taste a little salty. It has a thin silica sinter and occasionally emits a small gaseous plume.
Air Panas Balla -2 (APB -2)	796398	9675485	1586	93,1	7,8	0,06	7020	Hot spring appear among the altered boulders on the banks of the Balla River. The water is clear, smells slightly of sulfur and taste a little salty. Has a thin silica sinter around the hot spring.
Air Panas Balla -3 (APB -3)	796506	9675582	1623	47	5,3	0,006	231	Hot spring appear among the altered boulders on the banks of the Balla River. The water is clear, smells of sulfur and tasteless. It has a thin silica sinter and has a fairly large and continuous gas bubble.
Air Panas Balla -4 (APB -4)	796505	9675585	1621	59,2	3,5	0,20,	231	Hot spring appear among the altered boulders at the bottom of Balla River. The water looks a little cloudy, smells of sulfur is quite strong and has no taste. It has a thin silica sinter and continuous gas bubble.
Air Panas Balla -5 (APB -5)	796370	9675444	1585	93	8,1	0,02	9140	Hot spring emerge from rock fracture on the bank of the Balla River. The water looks clear, odorless and the water taste a little salty. The hot spring gave off a continuous gush of gas.
Air Panas Balla -6 (APB -6)	796379	9675467	1586	92,5	7,8	0,01	8320	Hot spring emerge from between boulders in the alluvium at the bottom of the Balla River. The water looks clear, odorless and water taste a little salty. The hot spring had a small but continuous gas plume.
Air Panas Balla -7 (APB -7)	796346	9675490	1586	93,3	8,2	0,04	8800	Hot spring arise from sand deposits of altered rock material on the banks of the Balla River. The water looks clear does not smell and the water tastes a little salty. The hot springs have a continuous small plume of gas.
Air Panas Balla – 8 (APB -8)	796477	9675573	1600	64,3	2,6	0,01	1110	Hot springs emerge from the crevices of altered rock on the banks of the Balla River. The water is clear, odorless, and slightly gritty. Occasionally emits small gas bubble and there is a thin sulfur deposit.
Air Panas Balla - 9(APB -9)	796451	9675566	1599	50,1	3,6	0,03	1890	Hot springs emerge crevices of altered rock on the banks of the Balla river. The water is a bit cloudy, smells a little of sulfur and feels a little gritty. Release gas bubbles and visible sulfur deposits
Air Panas Cepeng-1 (APC-1) *	797725	9671412	1256	37,6	6,3	1	2630	Hot springs emerge from pyroclastic rock crevices on the banks of the White River. The hot water is clear, taste sour, there are iron oxide deposits.
Air Panas Cepeng-2 (APC-2) *	797796	9671846	1269	39,8	5,9	2	1241	Hot spring emerge from pyroclastic rock crevices on the edge of the White River, the hot water is clear, tastes a little sour, there are iron oxide deposits.

*: Outside of the Survey Area and taken 2007

3. METHODOLOGY

3.1 Water classification

3.1.1 Cl-SO_4-HCO_3 ternary diagram

This diagram is used for the classification of thermal water based on the concentration of the three major anions Cl^-, SO_4^{2-}, and HCO_3^- which are plotted in a triangular diagram. In a volcanic setting, the major anions can give indications about the process by which the thermal water was formed. A typical grouping of waters is (i) volcanic waters and steam-heated waters (dominated by SO_4^{2-} which is formed by oxidation of H_2S from steam in oxygen-rich surface or shallow water), (ii) mixed or peripheral waters (dominated by HCO_3^-, formed by mixing of CO_2-rich steam with groundwater), and (iii) boiled geothermal reservoir fluid (dominated by Cl^- which may come from water-rock interaction). The Cl-SO_4-HCO_3 ternary diagram can be used to classify the geothermal waters accordingly. Steam-heated and other surface waters are not suitable for geothermometry (Giggenbach, 1988).

3.1.2 Cl-Li-B ternary diagram

The Cl-Li-B ternary diagram is used to trace the origin of thermal fluids. Lithium is used as a tracer for deep rock dissolution since it is the alkali metal least affected by secondary processes. The existence of lithium can be used as a reference for evaluating the possible origin of thermal waters based on the main conservative constituents of thermal waters, chloride and boron (Giggenbach, 1991). At high temperatures, Cl occurs largely as HCl and B as H_3BO_3. Both components are volatile and easily mobilized in high temperature steam. At low temperatures, HCl is converted by reactions with rock to the less volatile NaCl while B will remain in its volatile form to be carried in the vapour phase. The Cl/B ratio is often used to verify a common reservoir source for the waters, but care must be taken in applying such interpretation since waters from the same reservoir may show differences in this ratio due to lateral changes in lithology at depth (for example, the occurrence of a sedimentary horizon), or by the absorption of B into clays during lateral flow (Giggenbach, 1991).

3.1.3 Na-K-Mg ternary diagram

Giggenbach (1988) proposed the Na-K-Mg ternary diagram as a method to determine reservoir temperature and to classify waters into fully equilibrated, partially equilibrated, and immature waters with respect to minerals containing those cations. The classification acts as a guide to which waters are most suitable for geothermometry and to detect mixing trends. The “fully equilibrated water” is in equilibrium both with regard to the Na/K and K/Mg geothermometers and is therefore most useful for geothermometry. The partially equilibrated waters are less reliable as geothermometers and immature water can be excluded as geothermometers are based on equilibria of water-rock interaction.

3.2 Geothermometry

Silica geothermometers are based on experimentally determined and temperature dependent equilibria. Silica can be present in various forms in geothermal fields, such as quartz, cristobalite, chalcedony, or amorphous silica, that give rise to different geothermometers based on silica solubility of different silica species with respect to temperature and pressure. Silica geothermometers using different forms of silica have been calibrated with simple equations up to about 250°C. The solubility temperature curve departs significantly from linearity after that, including the quartz geothermometer by Fournier and Potter (1982) which is calibrated up to 900°C.

The quartz geothermometer is usually the most reliable for reservoir temperatures above 150°C. Below that temperature, chalcedony is likely to control the dissolved silica concentration. The quartz geothermometer may be problematic for reservoir temperatures from 230 to 250°C due to quartz being

dissolving and precipitating very fast at temperatures above about 230°C (Fournier, 1973). In the temperature range of 250-350 C, the silica geothermometer is the most useful when applied to waters produced from geothermal wells where movement from the reservoir to the surface is rapid.

Cation geothermometers are widely used to interpret compositions of water collected from hot springs. The Na/K geothermometer equation has a good level of accuracy if it produces a temperature in the range of 180-350°C. Calculation results that produce temperatures below 120°C are less reliable, because at that temperature the sodium and potassium concentrations are influenced by clay minerals and may no longer be controlled by ion exchange reactions in the feldspar (Nicholson, 1993). This geothermometer can be applied in neutral chloride spring water and equilibrated or partially equilibrated water. If the hot spring water is not of the chloride type and is not equilibrated, the SiO_2or Na-K-Ca geothermometers can be applied. The hot water samples included in this calculation is hot water of the chloride type, has a neutral pH, and is in partial equilibrium.

For this study, the quartz and chalcedony geothermometers were calculated using silica speciation from WATCH while the other geothermometers were calculated based on analytical results directly using the cation geothermometry equations in Table 2.

TABLE 2: Equations for water geothermometry

Geothermometer	Equation	Source
Quartz	$t = -42.2 + 0.28831S - 3.6686\,x10^{-4}\,S^{-2} + 3.1665\,x\,10^{-7}S^3 + 77.034\,logS$	Fournier and Potter (1982)
Chalcedony	$t = \frac{1032}{4.99 - logSiO_2} - 237.15$	Fournier (1977)
Na-K-Ca	$t = \frac{1647}{\log(Na/K)\ \beta\left[\log\sqrt{Ca}/Na) + 2.06\right] + 2.47} - 237.15$	Fournier and Truesdell (1973)
Na-K	$t = \frac{1390}{1.75 - \log(Na/K)} - 237.15$	Giggenbach (1988)
Na-Li	$t = \frac{1000}{0.389 - \log(Na/Li)} - 237.15$	Fouillac & Michard (1981)

For gas geothermometry, the equations of Arnórsson and Gunnlaugsson (1985) also Arnórsson et al. (1998) were used in this work (Table 3). The geothermometers chosen are the calibrations for gas ratios (CO_2/H_2, H_2S/H_2, H_2S/Ar and H_2S/Ar), assuming Cl > 500 ppm where necessary. All the equations utilized have been adjusted for adiabatic boiling to 100°C.

TABLE 3: Equations for gas geothermometry

Geothermometer	Equation	Source
H_2S/H_2	$t = 304.1 + 39.48Q$	Arnórsson and Gunnlaugsson (1985)
CO_2/H_2	$t = 311.7 + 66.72Q$	Arnórsson and Gunnlaugsson (1985)
H_2/Ar	$t = 0.640Q^2 + 43.260Q + 170$	Arnórsson et al. (1998)
H_2S/Ar	$t = 4.108Q^2 + 42.265Q + 137.6$	Arnórsson et al. (1998)

Q = log of gas ratio (in mmol/kg)

3.3 Mineral-solution equilibria

To anticipate reservoir temperature, geothermometers have been developed but different geothermometers can give different temperatures for the same reservoir. This could be due to the reservoir fluids mixing with cold water in the upflow zone, or it could be caused by variable reaction rates.

The best estimate of a reservoir temperature, according to Reed and Spycher (1984), can be obtained by evaluating the state of equilibrium between particular waters and various hydrothermal minerals as a function of temperature. As a result, if a set of minerals reaches equilibrium at a specific temperature, that temperature is most likely the reservoir temperature. The rising fluid has interacted with the rock. The ratio of the reaction quotient (Q) to the equilibrium constant (K) can be used to estimate the equilibrium state of minerals. The equilibrium constant and the reaction quotient are related to the Gibbs energy of reaction through Equation 2:

$$\Delta Gr = -RTlnK + RTlnQ = RTln\left(\frac{Q}{K}\right) \quad (2)$$

where Gr = Gibss free energy
R = the universal gas constant;
T = temperature (kelvin)
K = equilibrium state of minerals; and
Q = reaction quotient.

In a geothermal system, the ratio of the equilibrium constant (K) for a particular reaction to the reaction quotient (Q) can be used to determine the equilibrium state for that reaction. This can be used to assess the equilibrium state of a mineral and a solution (Arnórsson, 2000). Mineral saturation indices (SI) in aqueous solutions at various temperatures are calculated as follows:

$$SI = log\frac{Q}{K} = logQ - logK \quad (3)$$

where SI = Saturation index;
Q = reaction quotient; and
K = equilibrium state of minerals.

3.4 Stable isotopes

Isotope techniques detecting the hydrogen and oxygen isotope ratios of water and steam from geothermal fields are important tools for investigating the origin of geothermal waters. Craig (1963) demonstrated that geothermal fluids are mostly formed from meteoric waters.

In geothermal water research, the isotope ratios of $^{18}O/^{16}O$ and $^{2}H/^{1}H$ are useful as tracers of fluid origin as well as indicators of mixing and vapour separation processes. Normally, these isotope ratios are presented as a permille deviation from Vienna Standard Mean Ocean Water (VSMOW), using the so-called δ-notation.

The $\delta^{18}O$ value for meteoric waters at any locality is dependent upon latitude, altitude, and distance from the ocean (Nicholson, 1993). Samples from high latitudes and high elevation are lighter (more negative δ values). The δD and $\delta^{18}O$ values in precipitation have been used to construct the world meteoric line with the following expression (Craig, 1961):

$$\delta D = 8\,(\delta^{18}O) + 10 \quad (4)$$

The δD in geothermal water is found to be constant and often recharged far away (higher altitude). while the $\delta^{18}O$ may show a characteristic enrichment which is known as oxygen isotope shift which means that the $\delta^{18}O$ is higher (less negative) than that of the local meteoric water. This is due to oxygen isotope exchange with the surrounding rocks that are much richer in heavy isotopes. The degree of the isotope exchange depends on the amount of oxygen in the water and rocks, the initial $\delta^{18}O$ value, the water-mineral fractionation factor, the reaction time, and the surface contact area (Craig, 1963; Mainza, 2006).

3.5 WATCH program

The computer program WATCH version 2.4 (Arnórsson et al., 1982; Bjarnason, 2010) was used to calculate aqueous speciation from reported chemical component concentrations. Its principal application is in geothermal fluids, although it can also be used for non-thermal waters. The application reads chemical analyses of surface-collected water, gas, and steam condensate samples and computes the chemical composition of downhole, or aquifer, fluids at a temperature of choice. This includes pH, aqueous speciation, partial pressures of gases, redox potentials, and activity products for several minerals.

4. RESULTS

For the purposes of geothermal fluid analysis, hot water samples and selected cold water samples were chemically analysed for all main constituents as well as oxygen-18 and deuterium isotopes. Seventeen thermal samples from hot springs, warm springs, and cool waters were selected for the present geochemical study. Two samples were collected by the Geological Agency in 2007 and nine samples were collected in 2021 for a further investigation. All samples were analyzed at laboratory of Center for Mineral, Coal and Geothermal Resources, Bandung. The results of the analysis are shown in Appendix I, II, and III.(Iim et al., 2021)

Hot water sampling was carried out at 11 hot springs (Figure 3), namely APB-1, APB-2, APB-3, APB-4, APB-5, APB-6, APB-7, APB-8, APB-9, APC -1 and APC-2. This paper will focus on the Balla springs group and only mention Cepeng briefly.

Cold water sampling was carried out in 4 cold springs, namely ADB-5, ADB-6, ADB-7, and ADB-8. Four cold water samples were also obtained from river water, namely ADB-1, ADB-2, ADB-3, and ADB-4. There were 6 samples of gas obtained, namely GGB-1, water at the bottom of the Balla River GGB-3C, GGB-4, GGB-5 and GGB-6 hot springs.

Gas samples were also obtained from the cold spring gas bubble in the Kaipohan crater area, namely the Balla-6 (GGK) cold spring gas bubble. Finally, one gas sample was collected from a steam vent in the Balla alteration area, namely the northern part of Balla steam vent (GGB-2A). Results of analysis are presented in Appendix III.

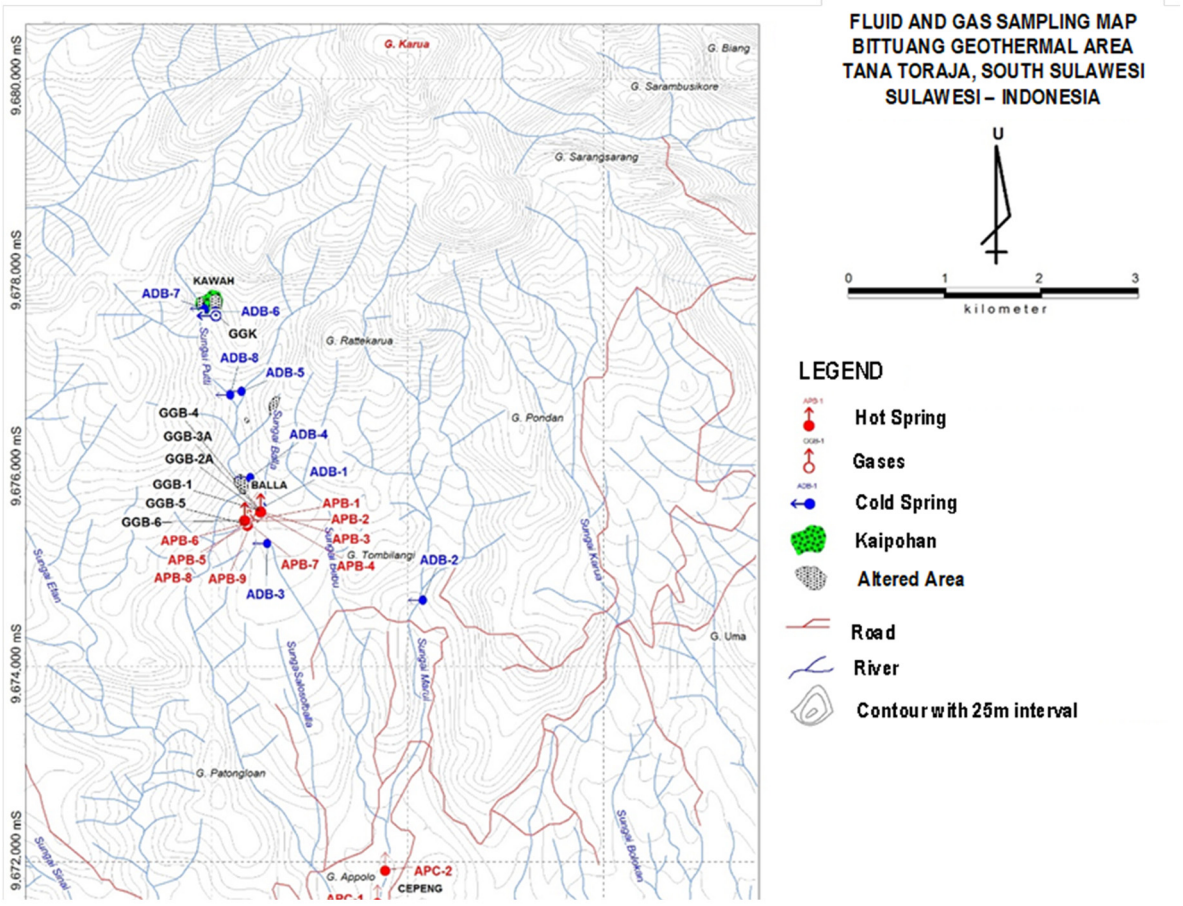

FIGURE 3: Fluid and gas sampling map of Bittuang (Suleman et al., 2021)

4.1 Water composition

In general, the concentration of anions and cations in the water samples is divided into 2 groups, namely the hot water group which has relatively higher anion and cation concentrations and the cold-water group which has relatively low anion and cation concentration.

To examine these further, selected parameters (T, pH, B, δD) were plotted against the concentration of chloride, which is a conservative component (Figure 4). Both conservative components (B, δD) show a similar mixing trend in which samples APB-5 and APB-7 appear to be closest to the geothermal endmember. Samples APB-6, APB-1, APB-2 and APB-9 also fall on the mixing lines whereas samples APB-3, APB-4, APB-8, APC-1 and APC-2 plot with the cold water. It is also apparent that the first group of samples has higher temperatures and pH than the other samples.

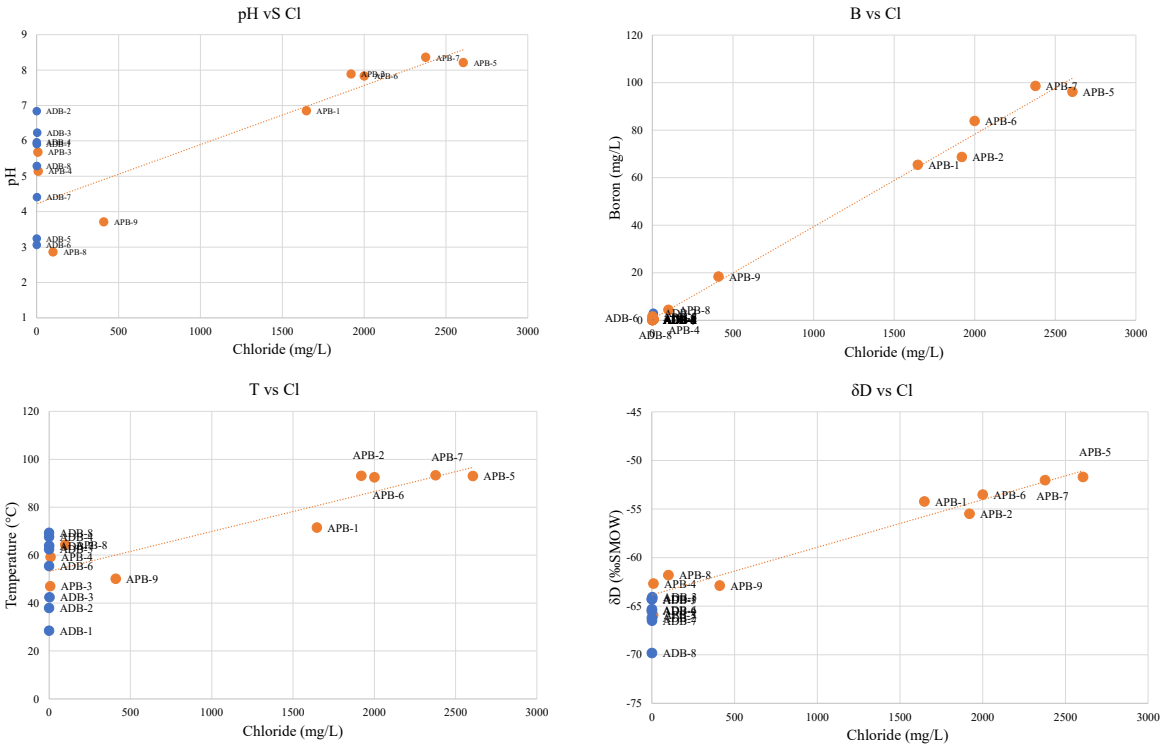

FIGURE 4: Relationship of temperature (T), pH, boron (B) and deuterium (δD) with chloride (Cl)

The anion concentrations of several hot waters on the Cl-SO_4-HCO_3 triangle diagram classify the water samples as chloride-type, chloride-sulfate and sulfate-chloride, sulfate-bicarbonate, and bicarbonate-type hot water (Figure 5).

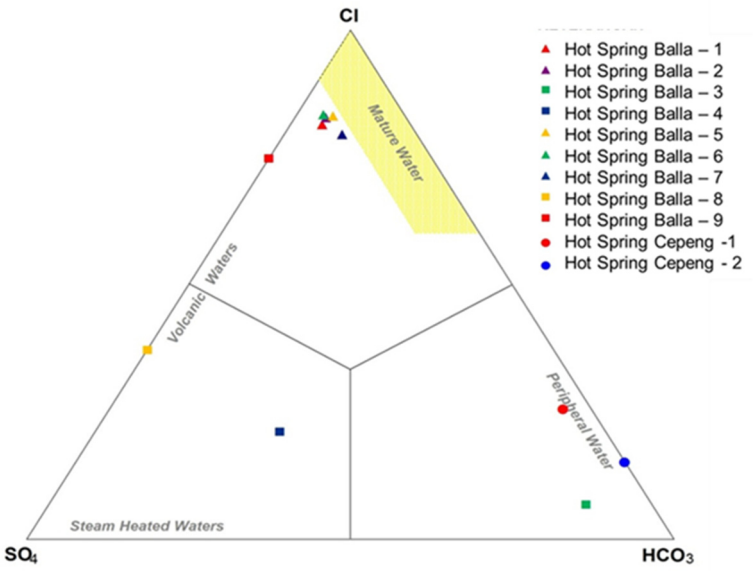

FIGURE 5: Cl-SO_4-HCO_3 ternary diagram for Bittuang thermal waters (Iim et al., 2021)

APB-1, APB-2, APB-5, APB-6, and APB-7 hot water are classified as chloride type waters. The five hot springs have higher concentrations of chloride (Cl) than sulfate (SO_4) and bicarbonate (HCO_3). The chloride concentration in the hot water ranges from 1600 mg/L to 2606 mg/L. Chloride water in hot springs at the surface indicates hot water originating from depth and high permeability zones such as fault zones. The pH of those samples is around 8. The other main elements in chloride water are sodium

(Na) and potassium (K) in a ratio of 10:1. The concentrations of Na, K, SiO_2 and B in APB-1, APB-2, APB-5, APB-6, and APB-7 hot springs are also high.

APB-8 and APB-9 plot as chloride-sulfate water with moderate concentrations of chloride and sulfate but no bicarbonate. Hot water of this type can be formed from magmatic fluids which contain volatile gases (CO_2, SO_2, HCl) that condense into a liquid phase, or by mixing of high-temperature geothermal steam and boiled geothermal water with shallow groundwater. Both processes would result in a low pH which is the case for those two samples (pH < 4). The reaction between acidic fluids and rocks that takes place near the surface will leach silica and metal cations (Na, K, Mg, Ca, Al, Fe) which can lead to high concentrations in the water.

APB-4 plots as a sulfate-bicarbonate type. The electrical conductivity and concentration of all three anions is much smaller than in the other hot waters, and the chloride concentration is close to the concentration in cold water. The pH is acidic. This water can therefore be presumed to be a result of condensation of geothermal steam mixed with meteoric water near the surface.

The water from APB-3 is of bicarbonate type. Such water contains a lot of CO_2 and is generally a product of the condensation process of gases and steam in surface water. For the APB-3 hot water, this is corroborated by an elevated concentration of bicarbonate, a moderate sulfate concentration, a low chloride concentration, and a relatively acidic pH (5.3).

The Cepeng-1 and Cepeng-2 bicarbonate waters are closer to the chloride area, with a higher concentration of chloride (Cl) than sulfate (SO_4). This suggests that the water contains a component of a chloride-type water which has been diluted by surface water mixed in with bicarbonate (HCO_3).

The results of the anion classification suggest that the samples from APB-1, APB-2, APB-5, APB-6 and APB-7 should be considered in greater detail as they most likely represent the geothermal fluid. The other samples are either steam-heated (APB-3, APB-4, APB-8, APB-9), mixed with surface water (Cepeng-1, Cepeng-2), or both.

The Cl-Li-B triangle diagram (Figure 6) shows that most Balla hot waters form a group which is in the middle of the triangle slightly shifted to the lithium (Li) corner. Only APB-8 and APB-9 hot springs are right in the middle while the rest are close to the rock composition. The concentration of Li in chloride-type hot water is very high, then gradually lowers to sulfate and bicarbonate-type hot water, suggesting mixing. If lithium is dissolved into the geothermal fluid, it does not easily react with other elements. The Li concentration is the same as in the chloride hot water which is estimated to come from the geothermal reservoir. However, due to mixing of geothermal fluid from the reservoir and meteoric water, the Li concentration in APB-8, APB-9, Cepeng-1, and Cepeng-2 is lower than the other samples.

APB-8 and APB-9 hot springs were originally thought to be chloride water of geothermal origin from deep below the surface. Because the water is in the Balla alteration area, the reaction between geothermal fluids and abundant clay minerals results in the acidic water which also has a high B/Li ratio of 14.5.
The arrangements of the hot spring samples in the Cl-Li-B triangle, which is in one cluster, is thought to be an indication of the similarity of the origin of the geothermal reservoir water from all the Balla hot springs. A comparison of Cl/B concentration mass ratios of all hot water samples shows very similar values ranging from 22 to 27. The low Cl/B ratio and clustering of the Balla hot spring samples near the rock part of the diagram suggests that the water has undergone extensive interaction with the rock (andesitic rock). This suggests that the APB-1, APB-2, APB-5, APB-6, and APB-7 hot springs are near or in the main upflow zone of the Bittuang geothermal system, whereas the Cepeng-1 and Cepeng-2 hot springs, which have a chloride component, might flow laterally from Balla before emerging in Cepeng.

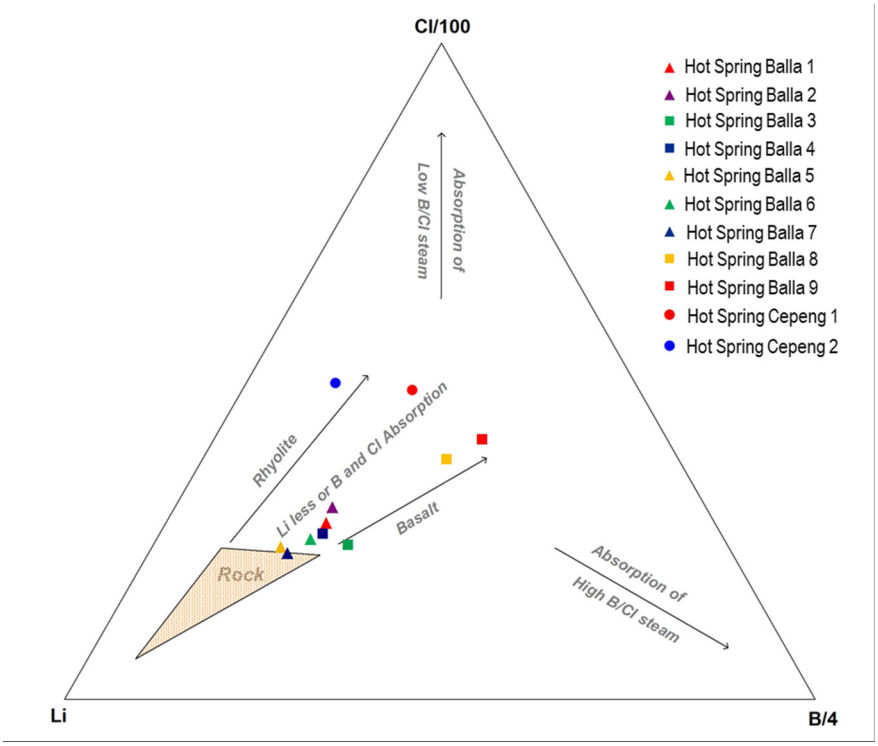

FIGURE 6: Cl-Li-B Ternary diagram for Bittuang thermal waters (Iim et al., 2021)

The triangular diagram of Na, K, and Mg (Figure 7) shows that APB-1, APB-2, APB-5, APB-6, and APB -7 hot water samples have cation ratios that suggest equilibrium between the geothermal fluid and feldspars. Meanwhile, APB-3, APB-4, APB-8, APB-9, Cepeng-1, and Cepeng-2 hot water samples appear to be immature water, i.e., they are not in equilibrium with rock.

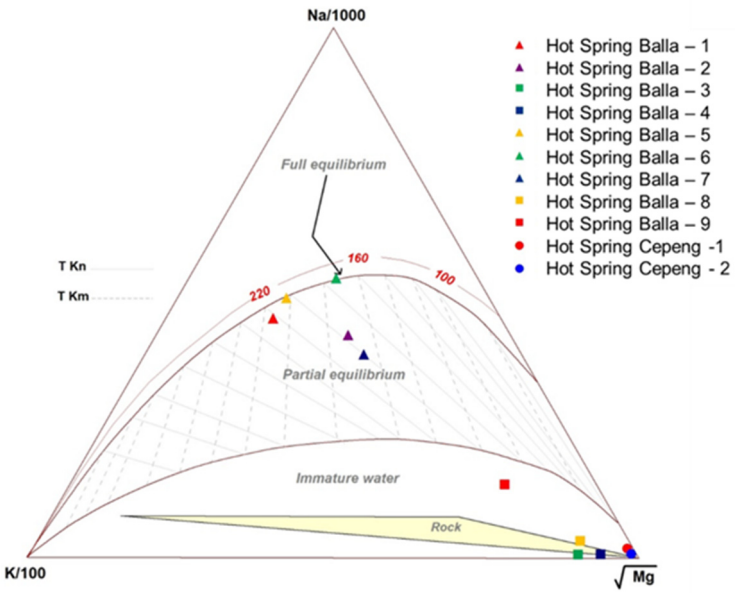

FIGURE 7: Na-K-Mg ternary diagram for Bittuang thermal water (Iim et al., 2021).

APB-1, APB-2, APB-5, APB-6, and APB-7 hot springs are in full or partial equilibrium. The samples in partial equilibrium may have mixed with meteoric water that enters the subsurface. This meteoric water also contains elements of Na and K, and an element of Mg. The Na and K elements from the reservoir will mix with the Na and K elements from the surface water, so it will affect the Na/K ratio,

in addition to a slight contamination with magnesium. However, for Bittuang the reservoir is more saline than the surface water which Na/K ratio will not be significantly affected by mixing with surface water. This causes lower concentrations for both Na and K but the ratio still reflects the reservoir conditions.

Hot water samples from APB-3, APB-4, APB-8, APB-9, Cepeng-1 and Cepeng-2 plot close to the corner of Mg or in the immature waters zone. This indicates that none of the hot water samples are in equilibrium with rocks. When there is no equilibrium in the hot water or when there is another process that causes changes in the concentration of these elements, it is impossible to estimate the subsurface temperature using the water.

As for the other classification methods, the cation ternary diagram suggests that APB-1, APB-2, APB-5, APB-6, and APB-7 show reservoir fingerprints and might be useful for geothermometry and fluid origin speculations. The other water samples are immature.

4.2 Gas composition

Figure 8 shows a ternary N_2-CO_2-Ar diagram that can be used to identify the origins of geothermal gases. Magma, sediments, the atmosphere, and meteoric water are all possible sources. The diagram shows the relative concentrations of CO_2, N_2, and Ar. CO_2 is the only one of these gases that is primarily geothermal in origin whereas N_2 and Ar are mostly atmospheric in origin (air and air saturated water: Giggenbach, 1987). The N_2/Ar ratio can be used to identify the atmospheric source; air saturated groundwater (ASW) has a N_2/Ar molar ratio of 38 while free air has a N_2/Ar molar ratio of 84 (Giggenbach, 1991).

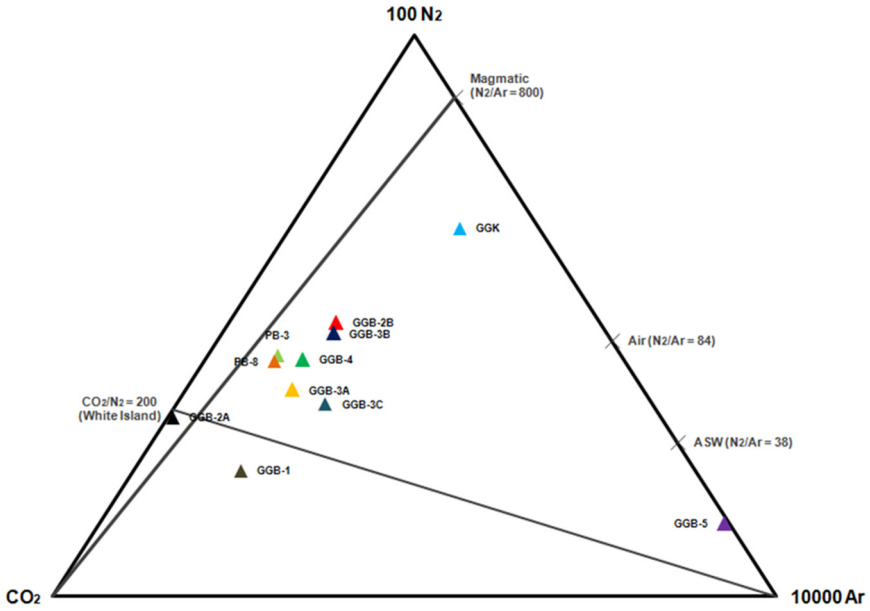

FIGURE 8: CO_2-N_2-Ar ternary diagram for Bittuang gas samples (Iim et al., 2021)

Giggenbach (1987) found that most of the gas samples from the volcanic system of White Island, which is fed by a magmatic source, had a CO_2/N_2 ratio of 200. This ratio was plotted where the N_2/Ar ratio (near the 800 line) and the Ar corner line intersect. Most of the Balla cluster gas samples shown characteristics of being of magmatic origin. The CO_2/N_2 ratios of GGB-1 and GGB-2A are 280 and 212, respectively. This might indicate that gas compositions of these gases are affected by a magmatic gas component.

4.3 Stable isotopes

Isotope analysis was carried out on 18 water samples from the Bittuang area, in particular isotope analysis of oxygen-18 (^{18}O) and deuterium (^{2}H). No steam or gas samples were analysed for stable isotopes. Based on the results of the analysis of the oxygen-18 and deuterium isotopes, values were obtained as shown in table in the Appendix IV. The oxygen-18 isotope content in APB-1, APB-2, APB-5, APB-6, and APB-7 hot springs appears to be almost 2 times greater than in the other water samples. The oxygen-18 isotope content in the five hot springs ranges from -5.7‰ to -4.0‰. It is suspected that in these 5 samples the interaction between geothermal fluids and rocks was more intensive, resulting in a much larger value of the oxygen-18 isotope or oxygen-18 enrichment. In addition, the deuterium isotope values in the 5 water samples appeared to be larger, between -55.5‰ to -51.7‰. Results of analysis are given in Appendix III.

5. DISCUSSION

5.1 Fluid origin

The graph of the relationship between the isotopes of oxygen-18 ($\delta^{18}O$) and deuterium ($\delta^{2}H$) with the global meteoric water line equation $\delta D = 8\ \delta^{18}O + 10$ is shown in Figure 9. The graph shows 2 groups of water samples, namely the hot water group which is on the right side of the local meteoric water line and hot water that are on the local meteoric water equation, i.e., together with the cold water. The hot water group on the right is hot water that has oxygen-18 isotope enrichment compared to meteoric water, namely APB-1, APB-2, APB-5, APB-6, and APB-7 hot springs. In addition, the five hot springs are also deuterium enriched compared to the other sample group. The position of the five hot springs is in the area around a mixing line, suggesting that there is a mixture of geothermal fluid and a more enriched water source, such as the subducted seawater termed “andesitic water” by Giggenbach (1993). The five hot springs move closer to the andesitic water box, suggesting gradually increasing mixing ratios.

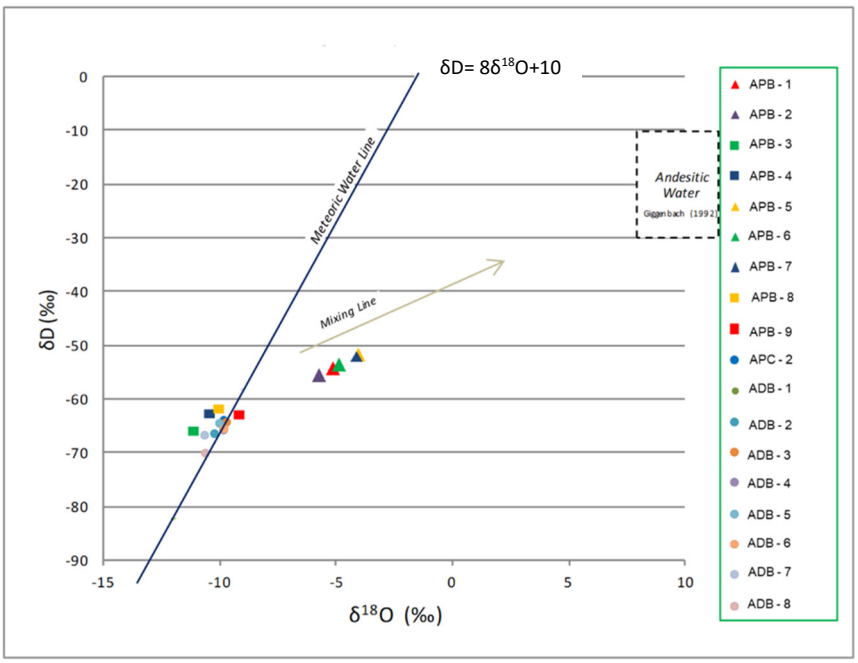

FIGURE 9: Stable isotope ratios in Bittuang geothermal waters

That the other hot and cold-water samples are almost exactly on the equation line of the local meteoric water is an indication that the water is of meteoric origin. This confirms the assumption that the five hot springs of chloride type that have undergone a partial equilibrium process are water from a deep geothermal reservoir with a high content of magmatic elements. The hot water in the remaining samples is meteoric water mixed with geothermal steam. Therefore, these five hot springs with chloride type water are more representative for the Bittuang geothermal reservoir water.

5.2 Reservoir temperature

Estimation of the subsurface temperature of the Bittuang geothermal reservoir is carried out using the method of calculating the solute geothermometer in the hot water sample and calculating the gas geothermometer from the gas samples.

The geothermometer used in this calculation are silica geothermometers and cation geothermometers. The dissolved elements used in the calculations are derived from chloride-type hot water samples with neutral pH from hot springs in Balla, i.e., samples APB-1, APB-2, APB-5, APB-6, and APB-7. The results are given in Table 4.

TABLE 4: Solute geothermometry calculations (°C)

SAMPLE	Quartz (Fournier and Potter, 1982)	Chalcedony (Fournier, 1977)	Na-K-Ca (Fournier and Truesdell, 1973).	Na/K (Giggenbach, 1988).	Li/Na (Fouillac and Michard, 1981).
APB-1	169	145	218	223	179
APB-2	165	141	200	195	169
APB-5	132	104	214	206	200
APB-6	136	109	177	167	183
APB-7	127	99	206	199	211

The calculation results based on the quartz geothermometer for the five chloride-rich samples from APB are in the range of about 130°C to 170°C. The chalcedony geothermometer gives systematically lower values, as expected, this is due to of the solubility of silica itself. However, the three cation geothermometers are in relatively good agreement, suggesting temperatures of 170°C to 220°C, with the most saline samples APB-5 and AP -7 suggesting reservoir temperatures of 200°C to 215°C.

Gas geothermometer calculations were also carried out to strengthen the reservoir temperature estimation, using the calibrations of Arnórsson and Gunnlaugsson (1985) and Arnórsson et al. (1998). The gas sample that is considered the best and closest to the actual condition at depth is GGB-2A gas sample, originating from the steam vent, which also has the highest CO_2 concentration. The other gas samples are not considered in the calculation due to the occurrence of gas bubbles through the water (fluid) or because the temperature is lower than the water boiling point. The results for the geothermometry calculation of GGB-2A using four different gas ratio geothermometers is presented in Table 5.

Based on this sample, gas geothermometry estimates the subsurface temperature of the Bittuang geothermal system to be between 250°C and 350°C.

The three geothermometer approach methods using quartz, cations and gas found different reservoir temperature values. The result from quartz geothermometry is 130-170°C, cations yield 200-220°C and gas geothermometers give 250-350°C.

TABLE 5: Gas geothermometer calculation results on Bittuang gas samples

GAS GEOTHERMOMETER	**GGB-2A** Temperatures in °C
H_2S/H_2	298
CO_2/H_2	247
H_2/Ar	291
H_2S/Ar	350

5.3 Mineral equilibrium

The WATCH 2.4 computer program (Arnórsson et al. 1982; Bjarnason, 2010) was used to calculate the aqueous speciation of geothermal fluids from the two hot springs richest in chloride (APB-5 and APB-7) based on the results of the chemical analysis of the samples with respect to an arbitrary reservoir temperature, either measured or obtained by a suitable geothermometer.

When geothermal fluids reach the surface, they cool due to conductive heat loss as they pass through cooler rocks or by boiling as the hydrostatic head decreases. The compositions of the ascending fluids vary because of each of these processes. While the cooling varies the degree of saturation with respect to both primary and secondary minerals and might therewith impact the estimated temperature. Conductive cooling can produce certain changes in the chemical composition of rising water through dissolution of minerals or precipitation. This is because the temperature drops and the degree of saturation varies where mineral dissolution or precipitation may occur. The boiling process also produces changes in the composition of the geothermal fluid that rises.

The log (Q/K) diagrams for APB-5 and APB-7, assuming conductive cooling, are shown in Figure 10. The minerals that are plotted in this diagram are calcite, adularia, anhydrite, albite, microcline, analcime, quartz, and chalcedony. The plots show that no best equilibrium temperatures can be found from this suite of minerals. APB-5 is at equilibrium with calcite at about 75°C while APB-7 is disequilibrium with calcite. So, to estimate the reservoir temperature, an intersection from other minerals is used. In this study the boiling graph did not show any intersection of minerals, but the cooling graph shows some minerals intersecting which means the equilibria point is reached.

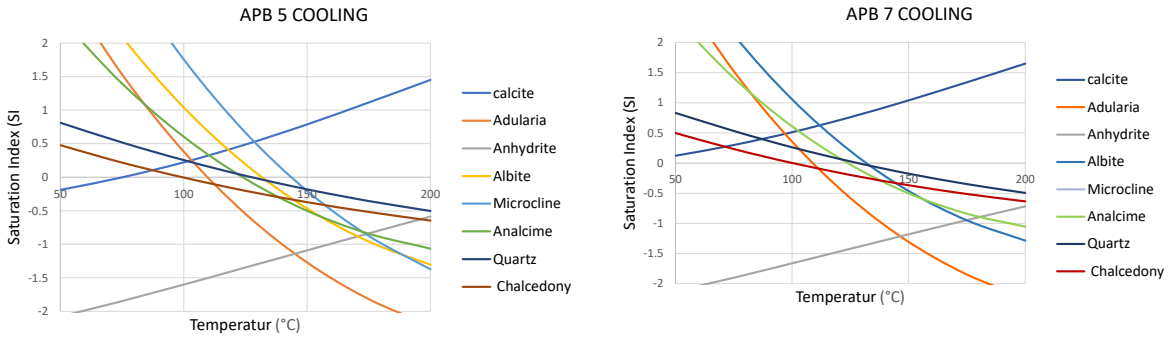

FIGURE 10: Mineral-solution equilibrium diagrams for Bittuang geothermal field

In sample APB-5, quartz, analcime and albite seem to reach equilibrium at 125°C while in APB-7, albite, analcime, quartz reach equilibrium at 130°C. That implies that subsurface temperatures of the field are in the range 100°C-130°C which covers the convergence points on the log (Q/K) diagrams corresponding to the mineral equilibrium point. This temperature range is close to the quartz geothermometry temperature which was estimated at around 130°C for these two samples (see Table 4).

Therefore (and as it was expected), the mineral-solution equilibria diagrams are reinforced by the silica geothermometers but not by the gas and cation geothermometers which give temperatures above 200°C. The reason for this is not clear, but one possibility might be that due to the very low flowrates of the host springs at Balla, the fluid has deposited minerals on its way to the surface and therefore the mineral saturation is not representative of the reservoir conditions. This possible explanation is reinforced by the presence of sintered silica at the hot springs.

6. CONCLUSIONS

The purpose of this report was to determine the type and origin of geothermal fluid samples and to estimate the subsurface temperature of the Bittuang geothermal area using the chemical composition of those samples. The conclusions of this study are as follows:

1. The presence of fumaroles and hot springs emitting boiled geothermal water suggests the presence of a geothermal system.

2. Cl-SO_4-HCO_3 and Na-K-Mg ternary diagrams characterise the waters from some of the hot springs at Balla as mature, chloride rich waters, plotting close in the area of mature geothermal fluids and in the partially equilibrated area. Other hot springs at Balla appear to be steam heated surface water, and bicarbonate springs are found at Cepeng.

3. The Bittuang geothermal system is a volcanic geothermal system. The hot springs APB-5 and APB-7 water samples were near-neutral pH, saline, and rich in chloride and boron. The isotope signature suggests intense water-rock interaction or mixing with an enriched component, e.g. “andesitic water”.

4. By considering the results of the subsurface temperature estimation approach with a dissolved element geothermometer and a gas geothermometer, the subsurface temperature of the Bittuang geothermal system is estimated to be 200–260 °C.

5. The hot springs at Cepeng probably represent outflow from the geothermal system.

7. SUGGESTIONS

With reference to detailed geological and geophysical surveys that have been carried out, further exploration is needed, such as slim hole drilling, to delineate the scope of the prospect area.

ACKNOWLEDGEMENT

I would like to thank the GRO-GTP for granting me this opportunity to participate in the 6-month training programme in Iceland. Special thanks go to Dr. Gudni Axelsson and staff members of GRÓ GTP, Ingimar, Markús, Málfrídur, and Dr. Vigdís for their assistance and arrangement in the past six months during the training programme and my stay in Iceland.

My sincere gratitude and acknowledgement go to Finnbogi Óskarsson, my advisor, for his guidance and knowledge of geochemistry, valuable advice and assistance during the writing of this report. My highest appreciation and gratitude go to all the lecturers for a variety of valuable lessons and their willingness to share their knowledge and experience, especially in geochemistry.

Finally, I want to acknowledge the Center for Mineral, Coal, and Geothermal Resources – Geological Agency, Ministry of Energy and Mineral Resources of Republic of Indonesia for their help, support and for allowing me to attend the 6-month training programme at the GRO-GTP. And my deepest thanks goes to my family for their support and encouragement during the period of the training programme.

To the 2021 GRO-GTP fellows, thank you for the friendship, the craziness, never ending laughing and sleepless night, see you when I see you.

REFERENCES

Arnórsson, S., 2000: Mixing processes in upflow zones and mixing models. In: Arnórsson, S. (ed.), *Isotopic and chemical techniques in geothermal exploration, development and use. Sampling methods, data handling, interpretation*. International Atomic Energy Agency, Vienna, 200-211.

Arnórsson, S., Sigurdsson, S. and Svavarsson, H., 1982: The chemistry of geothermal waters in Iceland I. Calculation of aqueous speciation from 0°C to 370°C. *Geochim. Cosmochim. Acta, 46,* 1513-1532.

Arnórsson, S., and Gunnlaugsson, E., 1985: New gas geothermometers for geothermal exploration – calibration and application, *Geochim. Cosmochim. Acta, 49,* 1307-1325.

Arnórsson, S., et.al 1998: New calibration for the quartz and Na/K geothermometers – valid in the range 0-350° C (in Icelandic). *Proceedings of the Geoscience Society of Iceland Annual Meeting,* April, 42-43.

Bachri, Sjaiful & Alzwar, Muzil, 1975: Laporan Inventarisasi Kenampakan Gejala Panasbumi Daerah Sulawesi Selatan (in Bahasa). Dinas Vulkanologi, Bagian Proyek Survei Energi Geotermal, Bandung

Bemmelem, van R.W.,1949. The Geology of Indonesia. Vol. IA The Hague Netherlands

Bjarnason, J.Ö. 2010: *The speciation program WATCH, version 2.4,* The Icelandic Water Chemistry Group, Reykjavík, 9 pp.

Craig, H., 1961: Isotopic variations in meteoric water. Science, 133, 1702-1703.

Craig, H., 1963: The isotopic geochemistry of water and carbon in geothermal areas. In: Tongiorgi, E. (ed.), *Nuclear geology on geothermal areas*. Consiglio Nazionale delle Ricerche, Laboratorio di Geologia Nucleare, Pisa, 17-53.

Fouillac, C. and Michard, G., 1981, Sodium/lithium ratios in water applied to geothermometry of geothermal reservoirs: Geothermics, 10, 55-70.

Fournier, R.O., 1973: Silica in thermal waters. Laboratory and field investigations. *Proceedings of the International Symposium on Hydrogeochemistry and Biochemistry, Tokyo, 1*, *Clark Co., Washington D.C.,* 122-139.

Fournier, R.O., 1977: Chemical geothermometers and mixing model for geothermal systems. *Geothermics, 5,* 41-50.

Fournier, R.O., and Potter, R.W., 1982: An equation correlating the solubility of quartz in water from 25° to 900°C at pressures up to 10,000 bars. *Geochim. Cosmochim Acta, 46*, 1969-1973.

Fournier, R.O., and Truesdell, A.H., 1973: An empirical Na-K-Ca geothermometer for natural waters. *Geochim. Cosmochim. Acta*, 37, 1255-1275.

Geological Agency, 2020: Indonesia's Geothermal Resources in 2020 (in Bahasa Indonesia). Badan Geologi, Bandung.

Giggenbach WF (1987) Redox processes governing the chemistry of fumarolic gas discharges from White Island, New Zealand. Appl Geochem 2:143–161

Giggenbach, W.F., 1988: Geothermal solute equilibria. Derivation of Na-K-Mg-Ca geoindicators. *Geochim. Cosmochim. Acta, 52*, 2749-2765.

Giggenbach, W.F., 1991: Chemical techniques in geothermal exploration. In: D'Amore, F. (coordinator), *Application of geochemistry in geothermal reservoir development*. UNITAR/UNDP publication, Rome, 119-144.

Giggenbach, W. F. (1993) Redox control of gas compositions in. Philippine volcanic-hydrothermal systems. Geothermics. 22, 479-519.

Iim, et al., 2021: *Final Report of the Detailed Geochemstry (PERTAGASTECH) Survey of the Bittuang Geothermal Area, Tana Toraja Regency, South Sulawesi Province* in Bahasa (unpublished report). Center for Mineral, Coal and Geothermal Resources, Bandung, 81pp.

Mainza, D., 2006: The chemistry of geothermal waters of SW-Uganda. Report 12 in: Geothermal training in Iceland 2006. UNU-GTP, Iceland, 219-244.

Nicholson, K., 1993: *Geothermal fluids: chemistry and exploration techniques*. Springer-Verlag, Berlin, 268 pp.

Radja, Vincent, 1970. Geothermal Energy Prospect in South Sulawesi. Power Research Indonesia. Jakarta.

Ratman, N., and Atmawinata, S., 1993: *Peta Geologi Lembar Mamuju, Sulawesi Skala 1:250.000*. Pusat Penelitian dan Pengembangan Geologi, Bandung.

Reed, M.H., and Spycher, N.F., 1984: Calculation of pH and mineral equilibria in hydrothermal water with application to geothermometry and studies of boiling and dilution. *Geochim. Cosmochim. Acta, 48*, 1479-1490.

Sutoyo, 2010: Karua Volcano In Bittuang Geothermal Area, Tana Toraja, South Sulawesi: One Of The Active Type B (?) In Indonesia (in Bahasa). Vol. 5 No. 1 (2010): *Buletin Sumber Daya Geologi.* Center for Geological Resources, Bandung.

Suleman, et al., 2021: *Final Report of the Detailed Geological Survey of the Bittuang Geothermal Area, Tana Toraja Regency, South Sulawesi Province,* in Bahasa (unpublished report). Center for Mineral, Coal and Geothermal Resources, Bandung, 110 pp.

APPENDIX I: Results of chemical analysis of hot water (APB) Bittuang Region

	Air Panas Balla-1 (APB-1)	**Air Panas Balla-2 (APB-2)**	**Air Panas Balla-3 (APB-3)**	**Air Panas Balla-4 (APB-4)**	**Air Panas Balla-5 (APB-5)**	**Air Panas Balla-6 (APB-6)**	**Air Panas Balla-7 (APB-7)**	**Air Panas Balla-8 (APB-8)**	**Air Panas Balla-9 (APB-9)**	**Air Panas Cepeng-1 (APC-1)***	**Air Panas Cepeng-2 (APC-2)***
pH	6,8	7,8	5,3	3,5	8,1	7,8	8,2	2,6	3,6	6,3	6,0
Conductivity (µs/cm)	4590	4620	151	90	6430	5370	6470	940	1349	2630	1241
SiO_2 (mg/L)	205,33	182,66	176,37	46,06	97,56	105,68	105,73	162,03	141,21	159,86	170,25
B (mg/L)	65,44	68,71	0,41	0,41	96,12	83,85	98,57	4,41	18,41	9,21	0,93
Al^{3+} (mg/L)	0,47	0,11	1,02	0,00	0,08	0,15	0,09	22,75	2,65	0,00	0,00
Fe^{3+} (mg/L)	0,17	0,02	0,11	6,66	0,04	0,04	0,04	13,99	2,90	4,73	3,09
Ca^{2+} (mg/L)	8,26	6,55	7,73	3,25	8,39	7,12	7,30	6,10	9,98	190,20	119,34
Mg^{2+} (mg/L)	0,15	0,62	1,95	1,08	0,30	0,23	1,79	1,83	2,85	105,60	45,90
Na^{+} (mg/L)	1057,30	1214,00	20,52	5,98	1776,60	1426,00	1496,40	40,80	291,72	210,96	65,68
K^{+} (mg/L)	93,45	73,20	12,26	4,26	124,67	55,70	95,87	8,33	32,39	13,30	4,56
Li^{+} (mg/L)	15,83	16,28	0,08	0,10	33,38	22,49	31,52	0,42	1,27	1,20	0,48
As^{3+} (mg/L)	10,00	10,00	0,00	0,00	10,00	10,00	2,00	1,00	4,00	0,00	0,00
NH_4^{+} (mg/L)	1,15	1,32	0,55	0,86	1,21	1,16	1,34	1,86	0,82	0,00	0,00
F^{-} (mg/L)	0,79	1,19	0,00	0,00	3,12	1,87	2,05	0,00	0,00	0,50	0,50
Cl^{-} (mg/L)	1647,51	1920,41	7,50	9,56	2606,27	2000,46	2376,77	99,95	410,38	376,40	105,11
SO_4^{2-} (mg/L)	274,72	286,75	11,10	22,81	346,08	299,14	343,55	168,92	138,02	60,33	4,00
HCO_3^{-} (mg/L)	99,57	111,22	91,82	12,93	181,05	98,28	268,98	0,00	0,00	998,25	592,94
$CO_3^{=}$ (mg/L)	0,00	0,00	0,00	0,00	0,00	0,00	0,00	0,00	0,00	0,00	0,00
Ion Balance (%)	2,1	3,5	2,9	0,4	1,4	2,4	4,0	3,7	2,1	0,2	0,6

* Taken in 2009

APPENDIX II: Results of chemical analysis of cold water (ADB) Bittuang Region

		Air Dingin Balla-1 (ADB-1)	Air Dingin Balla-2 (ADB-2)	Air Dingin Balla-3 (ADB-3)	Air Dingin Balla-4 (ADB-4)	Air Dingin Balla-5 (ADB-5)	Air Dingin Balla-6 (ADB-6)	Air Dingin Balla-7 (ADB-7)	Air Dingin Balla-8 (ADB-8)
pH		6,2	7,0	6,2	6,8	4,0	3,6	4,6	5,0
Conduct-ivity	(µs/cm)	42	65	30	58	222	312	237	194
SiO_2	(mg/L)	28,47	37,94	4 2,41	67,61	62,44	55,45	63,93	69,28
B	(mg/L)	0,12	0,12	0,12	0,12	1,64	0,12	0,12	0,12
Al^{3+}	(mg/L)	0,00	0,00	0,01	0,00	6,60	5,70	3,15	0,38
Fe^{3+}	(mg/L)	0,12	0,01	0,00	0,00	5,83	6,46	4,00	1,27
Ca^{2+}	(mg/L)	3,32	7,43	2,73	4,52	5,03	6,86	9,22	14,49
Mg^{2+}	(mg/L)	0,87	2,77	0,31	0,60	2,08	1,97	6,00	9,10
Na^{+}	(mg/L)	4,72	5,39	3,24	6,40	5,94	4,63	11,97	9,07
K^{+}	(mg/L)	3,53	2,72	2,05	5,88	4,05	3,26	8,59	4,91
Li^{+}	(mg/L)	0,06	0,07	0,06	0,07	0,06	0,06	0,09	0,07
As^{3+}	(mg/L)	0,10	0,00	0,00	0,00	0,00	0,00	0,00	0,00
NH_4^{+}	(mg/L)	0,49	0,60	0,38	0,42	0,87	0,59	0,81	0,91
F^{-}	(mg/L)	0,22	0,00	0,00	0,00	0,41	0,21	0,00	0,09
Cl^{-}	(mg/L)	0,41	0,19	3,00	0,11	0,23	0,17	1,09	0,38
SO_4^{2-}	(mg/L)	2,50	4,11	0,50	9,84	92,18	90,00	115,71	74,95
HCO_3^{-}	(mg/L)	29,74	47,85	15,52	31,04	0,00	0,00	0,00	46,55
$CO_3^{=}$	(mg/L)	0,00	0,00	0,00	0,00	0,00	0,00	0,00	0,00
Ion Balance (%)		5,0	3,4	1,6	2,0	3,5	4,0	3,0	4,5

APPENDIX III: The results of the chemical analysis of gas samples from the Bittuang geothermal area and the comparison values of several gases

GAS	SAMPLE CODE										
	GGB-1**	GGB-2A**	GGB-2B	GGB-3A	GGB-3B	GGB-3C**	GGB-4	GGB-5	GGK	PB-3*	PB-8*
Temperature (°C)	56	68.2	62,4	60,1	60,1	68,0	47,0	89,8	17,0	23,4	42,6
He (%mol)	-	-	0,0025	0,0028	0,0038	-	0,0029	ttd	0,0010	0,0010	0,0020
H_2 (%mol)	0,0425	0,0470	0,0430	0,0600	0,0770	0,0625	0,0300	ttd	ttd	0,0660	0,0690
O_2 (%mol)	-	-	0,0400	ttd	0,0160	-	ttd	3,4780	0,5210	0,0570	0,0460
Ar (%mol)	0,0024	0,0001	0,0040	0,0030	0,0040	0,0045	0,0030	0,0710	0,0190	0,0020	0,0020
N_2 (%mol)	0,3550	0,4690	1,3230	0,7500	1,2200	0,7490	0,9400	15,9760	5,5940	0,8940	0,8540
CH_4 (%mol)	0,0119	0,0014	0,0050	0,0060	0,0070	0,0018	0,0140	0,0210	0,0160	0,0020	0,0190
CO_2 (%mol)	99,5000	99,4000	98,5560	99,1283	98,5993	99,1000	98,9701	80,3032	93,4936	98,8800	98,8600
H_2S (%mol)	0,1240	0,0665	0,0255	0,0490	0,0725	0,0996	0,0404	0,1507	0,3553	0,0720	0,1450
HCl (%mol)	utd	utd	utd	0,0170	utd	utd	utd	utd	utd	utd	utd
NH_3 (%mol)	0,0256	0,0056	utd	utd	0,0005	0,0045	utd	0,0005	utd	0,0020	0,0030
N_2/Ar	150	4968	331	250	305	166	313	225	294	447	427
He/Ar	-	-	0,6	0,9	0,9	-	1,0	-	0,1	0,5	1,0
H_2/Ar	18	498	11	20	19	14	10	-	-	33	35
CO_2/Ar	42161	1052966	24639	33043	24650	21973	32990	1131	4921	49440	49430
CO_2/N_2	280	212	74	132	81	132	105	5	17	111	116

utd : undetected

* Sampling and analyzed by PSDMBP (Oktober, 2020))

** Analyzed by Thermochem (2021)

APPENDIX IV: The oxygen-18 and deuterium analysis result for hot and cold samples in Bittuang

SAMPLE	OXYGEN-18 ($\delta^{18}O$)	DEUTERIUM (δD)
	(‰)	(‰)
APB-1	-5,10	-54,22
APB-2	-5,70	-55,49
APB-3	-11,11	-65,94
APB-4	-10,42	-62,68
APB-5	-4,01	-51,70
APB-6	-4,85	-53,52
APB-7	-4,09	-52,03
APB-8	-10,02	-61,82
APB-9	-9,14	-62,89
APC-2	-9,82	-64,10
ADB-1	-9,76	-64,26
ADB-2	-10,24	-66,21
ADB-3	-9,72	-64,09
ADB-4	-9,85	-65,52
ADB-5	-10,02	-64,30
ADB-6	-9,83	-65,33
ADB-7	-10,66	-66,50
ADB-8	-10,63	-69,84